

Nanorheology of molecularly thin films of *n*-hexadecane in Couette shear flow by molecular dynamics simulation

A. Jabbarzadeh, J.D. Atkinson, R.I. Tanner *

Department of Mechanical and Mechatronic Engineering, The University of Sydney, Sydney, NSW 2006, Australia

Received 18 July 1997; received in revised form 22 September 1997

Abstract

In this work the rheological and structural properties of *n*-hexadecane have been studied by molecular dynamics simulation. The model consists of two structured atomic walls between which the fluid is sheared by moving the walls in opposite directions. The fluid consists of chains of *n*-hexadecane molecules. Each molecule has 16 interaction sites where each site on the molecule represents a CH₂ or CH₃ group. The Lennard–Jones potential governs the intermolecular interactions. Stretching, angular and torsional potentials are used for the intramolecular interactions to preserve the integrity of the molecules. An isothermal simulation of the Couette shear flow is conducted to reveal the rheological properties of *n*-hexadecane at high Weissenberg numbers in films as thin as 1 nm. The results obtained show an increase in the average viscosity of hexadecane as the film thickness is decreased to scales comparable to the molecular diameter of the chain segments. These results agree with recent experimental findings for very thin films, revealing shear thinning and normal stress difference effects which are an indication of non-Newtonian behaviour. Structural properties such as the density profiles, bond angle and dihedral angle distribution functions and average end-to-end distance of the molecules are obtained for films of different thickness and at different shear rates. The effects of the wall–fluid interaction strength on the fluid properties are also investigated in different adsorption limits. It seems that adsorption is a determining factor in the properties of these ultrathin films. The results indicate different shear responses depending on the adsorption limit of the surface. © 1998 Elsevier Science B.V. All rights reserved.

Keywords: *n*-Hexadecane; Nanorheology; Couette shear flow

1. Introduction

There has been extensive research in the area of thin liquid films. Understanding the behaviour of these ultrathin films has significant importance in many diverse areas of engineering and science applications such as spreading, wetting, lubrication, polymer coating and processing, friction and thin film casting. This fact has led researchers to develop both

* Corresponding author. Fax: + 61 2 93517060.

experimental and computational methods in the search for unexpected behaviour and properties of molecularly thin films.

Although the experimental work has revealed many intriguing properties of thin films [1–8], there are many questions that need to be answered by molecular analyses of these tiny systems. The rheological properties of thin liquid films have significant importance in many crucial areas of technology such as lubrication and polymer processing. It is believed that the shear response of a thin liquid film could be very different to that of the bulk liquid. In some lubrication problems, for instance in internal combustion engines, some parts experience tremendously high shear rates combined with high pressures and temperatures. It is imaginable that under these extreme conditions the thickness of the lubricating film could be comparable to the lubricant's molecular diameter. In such boundary lubrication conditions the Reynolds theory of lubrication breaks down [3]. The extreme conditions in some cases make it difficult if not impossible to measure the properties of interest of such thin films. The tiny scales and high shear rates in these conditions make molecular dynamics a natural approach for this class of problems. We note that there have been many molecular simulations [9,10] for simple spherical Lennard–Jones (LJ) particles. There have been few simulations of molecular liquids [11–13] and these were mainly concerned with the equilibrium properties of the confined liquid. The model chains in these simulations were ‘necklace’-like trains of a number of segments connected together by a strong potential. This model lacked the intramolecular architecture including the bond lengths, bond angles and dihedral potentials which are the natural part of real polymer molecules. This fact makes it difficult to decide if these ‘necklace’ chains will behave like real polymers [12].

One of the commonly used liquids in experiments [3–6] with thin liquid films is hexadecane, so computer simulations for thin films of hexadecane can be useful for comparison of the results.

There are some MD simulations reported for hexadecane in series of NEMD simulations of homogenous bulk hexadecane [14–17]. Hexadecane is a member of the alkane family and is a non-polar short chain molecule. Here we present the simulations for hexadecane in Couette shear flow geometry between structured atomic walls. We will present the simulation details and rheological results of hexadecane along with structural properties. We will also investigate the effect of the wall properties at low and high adsorption limits on the properties of the sheared liquid.

2. Simulation details

In this simulation the fluid is confined between two solid walls. These walls are parallel to the XY plane and Couette flow is generated by moving two walls in opposite directions along the X axis with the same speed so that shear is applied in the XZ plane. The fluid itself is a model polymer consisting of chain molecules. Each molecule has several interaction sites (‘atoms’). These interaction sites which we will refer to as atoms are actually CH_3 or CH_2 groups connected together making a chain. This kind of polymer model is widely used by researchers for simulation of alkanes [18], hexadecane [15,17] and polyethylene [20]. The model used for the polymer chain is an extension of the (RB) model developed by Ryckart and Bellemans [19]. The model includes angle bending, bond stretching and dihedral angle potentials. We have used chain molecules with 16 interaction sites as a model of hexadecane in our simulation. Fig. 1

shows a three dimensional picture of a hexadecane molecule as used in our simulation. In our simulation hexadecane with a reduced density of $2.288 \sigma^{-3}$ (810 kg m^{-3}) is sheared in an isothermal condition at a reduced temperature of $T_0 = 9.46\varepsilon/k_B$ (478 K).

Each wall is comprised of three layers of atoms of a BCC (body centred cubic) lattice. Each atom on the wall is attached by a stiff spring to its lattice position. The wall springs have a potential of the form

$$\phi_s = \frac{1}{2}k_w R^2, \quad (1)$$

where k_w is the stiffness of the spring and R is the distance between the wall atoms and their sites. Here a relatively soft wall spring with a stiffness of $k_w = 75\varepsilon\sigma^{-2}$ was used to overcome the slip problem [21]. The density of the wall atoms can be adjusted by packing them at different distances from each other. In our simulation we have used a wall density of $\rho_w = 2.5\sigma^{-3}$.

To overcome the penetration of the high density fluid particles into the walls at high shear rates a barrier wall [21] is employed in the form of

$$\phi = 0.0002\pi\varepsilon \left[\frac{2}{5} \left(\frac{\sigma}{z} \right)^{10} - \left(\frac{\sigma}{z} \right)^4 \right]. \quad (2)$$

This potential originally is the result of integration of a 6–12 Lennard–Jones potential on an XZ plane of an FCC lattice [22]. We have modified the original potential by removing the long range attractive part of the potential and making the potential much weaker. The potential and the force exerted on the fluid particles depend only on the normal distance of the fluid particles from the barrier wall. This potential has a very short range and is cut off at a distance of 0.2σ . It exerts only a normal force on the particles which are about to penetrate into the structured walls. This ensures that the barrier walls have the minimal possible effect on the fluid and only serves to solve some technical problems raised because of the high density and pressure of the simulated system [21]. The barrier walls are located 0.25σ deep inside the structured walls. This helps to reduce the slip and solve the penetration problem at the same time.

All the interactions between the atoms of different molecules and also interactions between the atoms which belong to the same molecule and are separated by more than three atoms are governed by a 6–12 Lennard–Jones potential described by

$$\phi_{IJ}(r) = 4\varepsilon \left[\left(\frac{\sigma}{r} \right)^{12} - \left(\frac{\sigma}{r} \right)^6 \right] - \phi_{\text{shift}}, \quad \phi_{\text{shift}} = 4\varepsilon \left[\left(\frac{\sigma}{r_c} \right)^{12} - \left(\frac{\sigma}{r_c} \right)^6 \right], \quad (3)$$

where r is the distance between two particles and ε and σ are the energy and length parameters of the potential. For hexadecane the values of $\varepsilon/k_B = 50.5 \text{ K}$ and $\sigma = 0.4045 \text{ nm}$ as recommended in [16] are used. The interaction between the structured wall particles and fluid particles

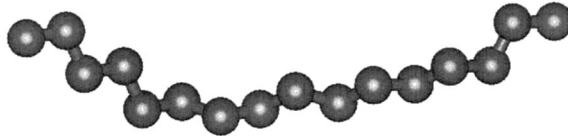


Fig. 1. A 3D picture of the hexadecane molecule with 16 interaction sites. Bond angle and dihedral angle potentials are included in this model.

is also governed by these equations with the wall length parameter $\sigma_w = \sigma$ but with ε replaced by ε_w which governs the strength of interaction between the walls and fluid.

The flexibility of the chains is restricted by a bond stretching potential $\phi(r)$, a bond angle potential $\phi(\theta)$ and a dihedral (torsional) potential $\phi(\alpha)$. The stretching potential $\phi(r)$ is described by

$$\phi(r) = \frac{1}{2} k (r_{ij} - r_0)^2, \quad (4)$$

where r_{ij} is the distance between the consecutive atoms of the same molecule and r_0 is the equilibrium distance or the bond length. The extensional stiffness k is a constant that depends on the type of molecules. Here $k = 51600 \varepsilon \sigma^{-2}$ is used for hexadecane. The angle potential has the form

$$\phi(\theta) = \frac{1}{2} k_\theta (\cos \theta - \cos \theta_0)^2, \quad (5)$$

where θ_0 is the equilibrium bond angle. Bending stiffness k_θ is a constant that depends on the type of molecule. Here $k_\theta = 868.6\varepsilon$ is used. The dihedral potential is described by

$$\phi(\alpha) = \sum_i^5 C_i (\cos \alpha)^i, \quad (6)$$

where $C_0 = 9.2789$, $C_1 = 12.1557$, $C_2 = -13.1201$, $C_3 = -3.0597$, $C_4 = 26.2403$, $C_5 = -31.4950$. These coefficients are in (kJ mol^{-1}) [23]. The equilibrium bond length and bond angle for hexadecane are $\theta_0 = 109.53^\circ$ and $r_0 = 0.153 \text{ nm}$ [16].

The equations of motion for the fluid and wall particles are

$$\dot{\mathbf{r}}_i = \frac{\mathbf{p}_i}{m}, \quad \dot{\mathbf{p}}_i = \mathbf{F}_i. \quad (7)$$

The isothermal condition is achieved by ad hoc rescaling of the thermal component of the velocities in all three directions according to the following equation

$$\beta^2 = (3Nk_B T_0) / \sum_{i=1}^N m_i (\mathbf{v}_i - U_i)^2, \quad (8)$$

where β is the rescaling factor by which all the thermal components of the velocities are rescaled. U_i is the flow velocity and \mathbf{v}_i is the laboratory velocity of the particle that is measured with respect to a fixed set of coordinates. k_B is the Boltzmann constant and T_0 is the set temperature. In our problem we have only flow or streaming velocity in the X direction. Some of the generated heat in the fluid is absorbed by the wall particles though rescaling of the thermal components of the velocities every few time steps makes sure that the fluid temperature remains constant. The wall particles are also thermostatted in the same way.

The streaming velocity is evaluated by dividing the whole region of the simulation volume between the walls into a sufficient number of bins. The number of bins is adjusted so that the thickness of each bin is 0.1σ in the Z direction. We add the X components of the velocities for the particles in each bin and then average it over the number of particles in that bin at each time step. Finally velocity profiles can be obtained by computing the time average velocity for each slice during the course of simulation. Thus the average velocity for each slice can be described as

$$U_{av,s} = \left\langle \frac{\sum_{i=1}^{N_f} u_{ix} N_s(Z_i(t))}{\sum_{i=1}^{N_f} N_s(Z_i(t))} \right\rangle, \text{ provided } \sum_{i=1}^{N_f} N_s(Z_i(t)) > 0, \quad (9)$$

where $U_{av,s}$ is the time average streaming velocity for each slice and u_{ix} is the X component of particle i 's velocity, N_f is the number of fluid atoms and angled brackets denote the usual time average. $N_s(Z_i(t))$ is a counting operator which is described by

$$\begin{cases} N_s(Z_i(t)) = 1 & \text{if } (s-1)\Delta Z < Z_i < s\Delta Z, \\ N_s(Z_i(t)) = 0 & \text{otherwise;} \end{cases} \quad (10)$$

it simply counts the number of the particles which happen to be in that particular slab at time t . There are some occasions when there is no fluid particle in some of the slices. This may result in a numerical error caused by zero divided by zero operation. Special care should be taken to avoid this situation and also to ensure that the results are statistically correct. In doing so Eq. (9) will be evaluated over the time steps when the accumulator for $N_s(Z_i(t))$ is greater than zero in the denominator of Eq. (9). Other local quantities such as density and temperature can be calculated in a similar way. The results of the streaming velocity profile then are fitted to a fifth order polynomial according to the following equation

$$U_x(z) = \sum_{k=1}^5 C_k z^k. \quad (11)$$

In the simulations here we run the program for a long time (100 000–500 000 time steps) until the velocity profiles are obtained and then use them for our calculations. The equations of motion are integrated by a leapfrog Verlet algorithm with a time step of 0.001–0.002 in reduced units depending on the shear rate.

The simulations are performed by a parallel algorithm [24] on a cluster of DEC Alpha 500/286 workstations by using PVM (Parallel Virtual Machine) message passing software that provided good speedup and efficiency.

2.1. Stress tensor

Stress tensor components were found for a microscopic system of particles by the Irving–Kirkwood (1950) method. According to this method the contribution of each particle to the stress tensor is in two parts, a configuration part and a kinetic part. This can be written as

$$\sigma_{\alpha\beta} = -\frac{1}{V} \left\langle \sum_i^N m_i u_{i\alpha} u_{i\beta} + \sum_i^N \sum_{j>i}^N \mathbf{r}_{ij\alpha} \mathbf{F}_{ij\beta} \right\rangle. \quad (12)$$

The first sum in the right hand side of Eq. (12) denotes the kinetic contribution where m_i is the atomic mass and α and β are coordination system axes which for a Cartesian system can be simply substituted by X , Y or Z , and $u_{i\alpha}$ and $u_{i\beta}$ are the peculiar velocity components of particle i in the α and β directions. The second sum represents the configuration or potential contribution where $\mathbf{r}_{ij\alpha}$ is the α component of the distance vector between particles i and j and $\mathbf{F}_{ij\beta}$ is the β component of the force exerted on particle i by particle j . However, in the case of

Table 1

Shear stress calculated from wall by Eq. (14) and from the Irving–Kirkwood relationship by Eq. (13) for a film thickness of 3.898 nm at various shear rates. For all the data points $\varepsilon_w = 4\varepsilon$

$\log \dot{\gamma}$ (s ⁻¹)	10	10.5	11	11.5	12
σ_{xz} (MPa)	11.416 ± 0.329	26.532 ± 0.824	54.904 ± 0.676	108.576 ± 0.768	246.860 ± 1.040
$\sigma_{xz,w}$ (MPa)	13.172 ± 0.297	28.032 ± 0.980	56.290 ± 0.957	109.816 ± 0.854	248.360 ± 1.490

molecular liquids the force term $\mathbf{F}_{ij\beta}$ will consist of both the LJ intermolecular interactions and also the intramolecular interactions which are due to the bond stretching, bond angle bending and dihedral potentials. In the algorithm, the contribution of the intermolecular and intramolecular interactions are calculated separately at each time step and then are added together. We have to exclude the mean flow velocity when we consider the laboratory velocity component of a particle in the flow direction. Then for shear stress we can rewrite Eq. (12) as

$$\sigma_{xz} = -\frac{1}{V} \left\langle \sum_i^N m_i u_{iz} [u_{ix} - U_{x,i}] + \sum_i^N \sum_{j>i}^N \mathbf{r}_{ijz} \mathbf{F}_{ijx} \right\rangle, \quad (13)$$

where $U_{x,i}$ is the average flow velocity at the position of particle i . It is evaluated from the Z coordinate of the particle and Eq. (11). The angle brackets denote the time average.

As a test of accuracy of Eq. (13) for calculation of shear stress we computed the time average of the force in the X direction applied to the wall particles by fluid particles during the simulation. Then we calculated the shear stress by dividing this force by the area of the walls. This shear stress is given by Eq. (14)

$$\sigma_{xz,w} = \sum_i^{N_w} \sum_j^{N_F} \mathbf{F}_{ij} / A. \quad (14)$$

The results for shear stress using Eqs. (13) and (14) proved to be in good agreement. To show this agreement the results for shear stress are calculated from Eqs. (13) and (14) for a film thickness of 3.898 nm at various shear rates and are displayed in Table 1.

It can be seen the agreement is good and in most cases the difference is only within the range of statistical uncertainties. We have used Eq. (12) for calculation of the stress tensor elements for all the results presented in this work.

2.2. Viscosity and material functions

The shear rate is slightly different at different distances from the wall because the gradient of the velocity is not constant along the z axis, therefore the local viscosity will be slightly different. More useful is the average over the whole width of the slit. Thus we use the following constitutive equation to find the viscosity

$$\eta = \frac{\sigma_{xz}}{\dot{\gamma}}. \quad (15)$$

For a rheologist, some interesting and important properties to measure and examine are the normal stress differences. The first and second normal stress differences are

$$N_1 = \sigma_{xx} - \sigma_{zz}, \quad N_2 = \sigma_{zz} - \sigma_{yy}. \quad (16)$$

We are using the normal sign convention of mechanics [25], so that a positive sign represents tension. Normal stress differences for Newtonian fluids are zero but non-Newtonian fluids exhibit normal stress difference effects.

3. Results

The results in this section will be presented for material functions and the structural properties of hexadecane. The results are organised for two categories of simulations that are conducted here namely for strongly and weakly adsorbing surfaces. With an strongly adsorbing surface the wall–fluid interaction strength parameter $\varepsilon_w = 4\varepsilon$. This value is considered to be in a range suggested [7] for mica surfaces which are used in experimental measurement. The second class of surface studied here has a lower value of $\varepsilon_w = \varepsilon$ for the wall–fluid interaction strength parameter. This surface is considered a weakly adsorbing surface.

3.1. Strongly adsorbing wall

3.1.1. Viscosity and film thickness

Simulations were performed for various hexadecane films with thicknesses ranging from 0.975 to 19.492 nm. The shear rate for all the simulations was $10^{11.5} \text{ s}^{-1}$ and wall–fluid interaction strength was $\varepsilon_w = 4\varepsilon$. The density of the film was the same for all the simulations and this was achieved by putting different numbers of molecules in the simulation box. The number of the fluid molecules and fluid segments and also the number of the wall atoms for different film thicknesses are given in Table 2. The results for the viscosity against the film thickness are displayed in Fig. 2. It can be seen from these results that the viscosity is not changing much with the film thickness down to a thickness of 0.975 nm where a sudden jump in the viscosity is observed. At this thickness however, there is some slip between the wall and fluid layers that can be seen from the velocity profiles for this film thickness in Fig. 3. This implies that without slip an even larger increase in the viscosity could be expected. A similar jump in the magnitude of the viscosity occurs in experiments. This jump is measured at about 0.8 nm by Van Alsten and Granick [5]. Although the experimental measurements were at much lower shear rates and temperatures our result is in qualitative agreement with their finding.

Table 2
Number of the fluid and wall atoms for different film thicknesses

Film thickness (nm)	0.9746	1.949	2.924	3.898	4.873	5.848	6.822	19.492
Number of fluid molecules	24	48	72	96	480	576	672	1920
Number of fluid segments	384	768	1152	1536	7680	9216	10 752	30 720
Number of wall atoms	528	528	528	528	2016	2016	2016	2016

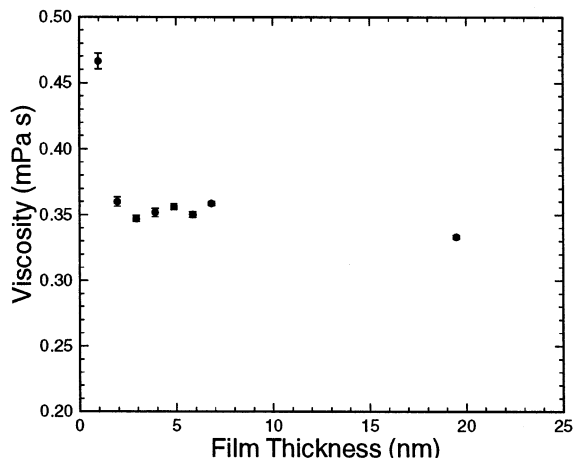


Fig. 2. Viscosity against film thickness for various film thicknesses ranging from 0.975 to 19.492 nm. Viscosity was measured at a shear rate of $10^{11.5} \text{ s}^{-1}$ for all the films. Wall–fluid interaction strength was $\varepsilon_w = 4\varepsilon$.

3.1.2. Non-linear shear response

To examine the shear response of hexadecane thin films, computations were made at shear rates between $10^{9.5}$ and $10^{12.5} \text{ s}^{-1}$. The lower shear rates were not simulated because of the long runs needed to extract the streaming velocity profiles and the average properties. The shear response was examined for four films with thicknesses 0.975, 1.949, 2.924 and 3.898 nm. These thicknesses are roughly equal to 2.5 to 10 segment diameters of the hexadecane molecule. Viscosity against shear rate is plotted in a logarithmic scale for all the four films in Fig. 4. It can be clearly seen from this figure that shear thinning happens and a non-Newtonian behaviour is observed for this range of shear rates. It can be seen that the viscosity obeys a power law in the form of $\eta = A\dot{\gamma}^{-\alpha}$. The exponent α depends on the thickness of the film and is given in Table

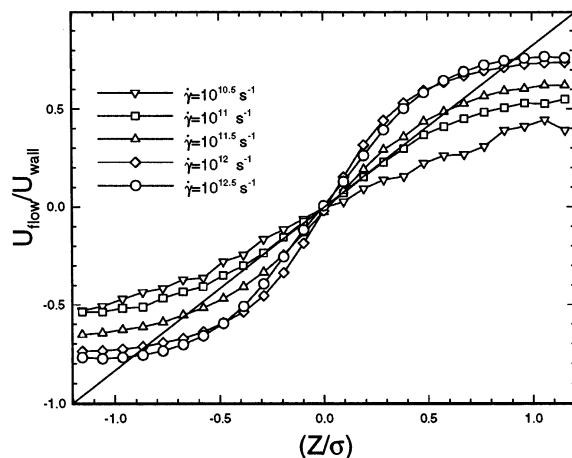


Fig. 3. The velocity profiles for a film with a thickness of 0.975 nm at various shear rates. Wall–fluid interaction strength was $\varepsilon_w = 4\varepsilon$.

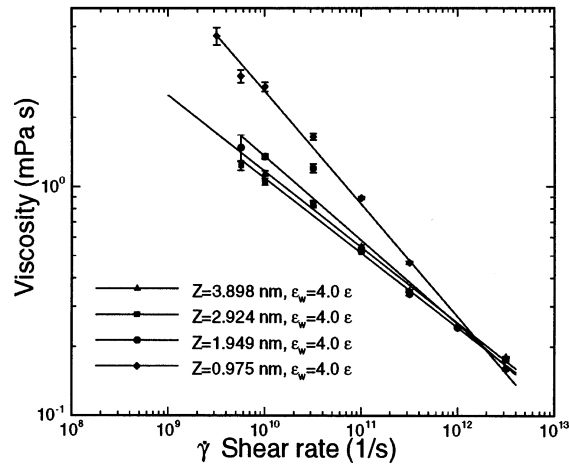


Fig. 4. Shear response of thin films of hexadecane for film with a thickness of 0.975, 1.949, 2.924 and 3.898 nm. The shear rate was in the range of $10^{9.5}$ to $10^{12.5}$ s^{-1} while the wall–fluid interaction strength was $\epsilon_w = 4\epsilon$.

3 for the films examined. It can be seen that the value of α is about $1/3$ for thicker films. Decreasing the film thickness results in an increase in α and eventually it changes to about $1/2$ at the thinnest film of 0.975 nm.

The dependence of α on the film thickness is in agreement with the experimental measurements for thin films of dodecane which is also a short chain molecule [8]. In experiments with hexadecane for a film thickness of 2.4 nm by Carson et al. [6] the shear thinning effect is also observed where α was about $1/2$ which is very close to α for the thinnest film from our simulation. The measurements for a dodecane film with a thickness of 2.7 nm also indicated shear thinning with viscosity obeying a power law, however, the measured value for the exponent α was slightly less than $2/3$ [8]. Their measurements were at a lower temperature and over a lower range of shear rates of at most 10^5 s^{-1} . The experimental measurements for liquid lubricants at high pressures and shear rates up to 10^4 s^{-1} by Bair [28] for polybutene in mineral oil gives a value of 0.35 for the exponent in the power law behaviour region. These measurements by Bair were conducted for much thicker films of 9.7 μm and the exponent agrees much better with the thicker film simulated here.

The results for the shear rates examined here are well into the non-Newtonian regime so a reliable estimate of the zero shear rate viscosity η_0 is not possible, but is expected to be many orders larger than that of the bulk hexadecane.

The simulated critical shear rate for the bulk hexadecane is about $\dot{\gamma}_{cr} \approx 10^{10}$ s^{-1} [14]. The relaxation time is estimated to be much less than 10^{-10} s [5], and since the viscosity of the bulk

Table 3

The dependence of α to the film thickness in the power law behaviour of viscosity given by $\eta = A\dot{\gamma}^{-\alpha}$

Film thickness (nm)	0.975	1.949	2.924	3.898
α	0.491	0.365	0.316	0.302

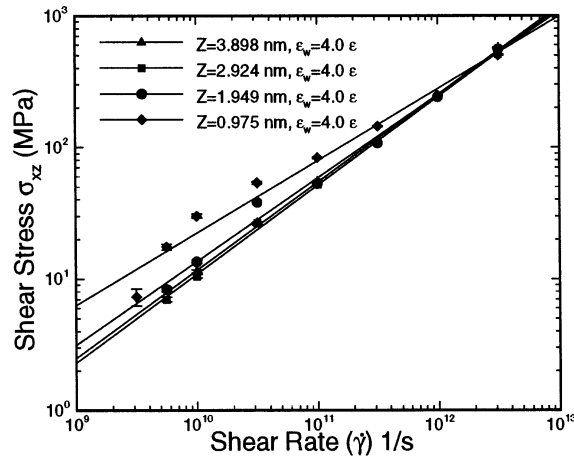


Fig. 5. Shear stress against shear rate in a logarithmic plot for film thicknesses of 0.975, 1.949, 2.924 and 3.898 nm. The wall–fluid interaction strength parameter was $\epsilon_w = 4\epsilon$.

hexadecane is about 0.003 Pa s at 25°C and 0.1 MPa pressure we can estimate the shear rigidity of the bulk fluid as being around 3×10^7 Pa. Hence all of our simulations are at high (> 1) Weissenberg numbers. In fact the characteristic Rouse relaxation time of polymers is [26,27]

$$\tau = \frac{6\eta_0 M}{\pi^2 \rho RT}, \quad (17)$$

where M is the molecular weight, ρ is density, R is the gas constant and T is temperature. In thin films being dealt with the effective η_0 is not known and the Eq. (17) can not be used. If η_0 is taken to be 0.003 Pa s for bulk hexadecane then the relaxation time of 10^{-10} s will be obtained from the Eq. (17). However, experiments with thin films of hexadecane [5,6] and dodecane [8] show much increased viscosities and relaxation times. For example dodecane in films of thickness 3.4–2.6 nm shows relaxation times of 10^{-2} – 5×10^{-2} s [8]. The viscosity for hexadecane can increase up to 25 Pa s [5]. These factors all increase the effective Weissenberg number seen in our calculations probably up to 10^4 times the values given from bulk properties.

So the expected critical shear rate for these thin films of hexadecane should be about 10^6 s $^{-1}$ and even much lower. This confirms that the results simulated here are well into the non-Newtonian regime.

3.1.3. Shear stress

The shear stress was also examined over different shear rates across film thicknesses of 0.975, 1.949, 2.924 and 3.898 nm. The results are plotted in Fig. 5 on a logarithmic scale. It can be seen that the shear stress has an increasing trend with shear rate. Shear stress like viscosity obeys a power law in the form of $\sigma_{xz} = A\dot{\gamma}^\alpha$. The dependence of α on the film thickness can be seen from Table 4 where α is given for various film thicknesses. The value of α is almost identical for thicker films of 2.924 and 3.898 nm, though for the thinnest film it is about 1/2. Theoretical analysis by Subbotin et al. [29] for polymer melts confined between strongly adsorbing solid walls which are separated by distances comparable to the radius of gyration of the chain

Table 4

The exponent α for various film thicknesses in the power law behaviour of shear stress given by $\sigma_{xz} = A\dot{\gamma}^\alpha$

Film thickness (nm)	0.975	1.949	2.924	3.898
α	0.550	0.635	0.674	0.670

molecule predict this power law behaviour for shear stress in planar Couette shear flow. They predicted different values for α depending on the shear rate. For higher shear rates they predicted α to be $1/2-1/3$. This clearly is more in agreement with the results for the thinnest film of 0.975 nm.

3.1.4. Normal stress differences

3.1.4.1. First normal stress difference N_1 . In experiments with thin liquid films no report has mentioned the normal stress differences. The reason for that might be the technical difficulties in measuring these properties for such thin films. This is not so difficult in the simulation once one sets up a proper model and starts the simulation. The normal stress differences N_1 and N_2 can be calculated from Eq. (16). Fig. 6 shows the first normal stress difference against the shear rate for films with thicknesses of 0.975, 2.924 and 3.898 nm. It can be seen from this figure that at lower shear rates up to $10^{10.5}-10^{11} \text{ s}^{-1}$, N_1 is negative. This abnormal behaviour for N_1 is an indication of strong attraction between the two surfaces. This attractive force has been observed in experiments with different liquids, including hexadecane in measurement of the force between the surfaces by Christenson et al. [4]. They observed this attraction by a jump inward between the surfaces when they were brought close together. This jump inward happened for hexadecane at a distance of about 5–6 nm.

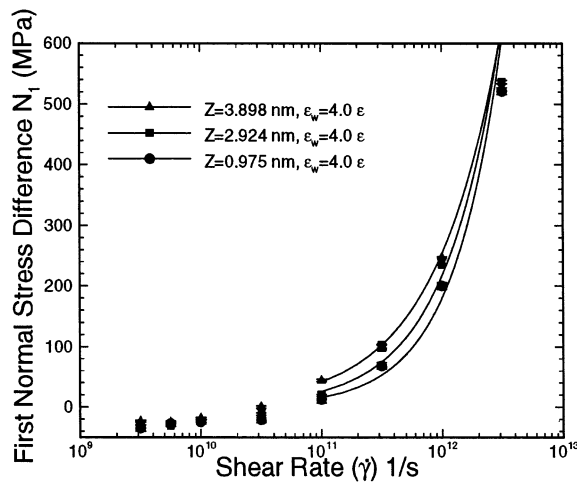


Fig. 6. First normal stress difference against the shear rate. The results here are for three different film thicknesses. Wall–fluid interaction strength was $\epsilon_w = 4\epsilon$. The error bars are all smaller than the symbols and can not be seen clearly in the graph. Typical statistical error is 1–3 MPa.

Table 5

The dependence of α to the film thickness in the power law behaviour of N_1 given by $N_1 = A\dot{\gamma}^\alpha$

Film thickness (nm)	0.975	2.924	3.898
α	1.058	0.926	0.785

The films examined in our simulations are also within this attractive range. However, at higher shear rates the value of N_1 changes to positive and rapidly increases in magnitude as the shear rate is increased. In Fig. 6 the positive values of N_1 are fitted to an exponential curve. The results shows that N_1 obeys a power law similar to that observed for viscosity in the form $N_1 = A\dot{\gamma}^\alpha$. However, the exponent in this case is positive and has a different value depending on the thickness of the film. The values for α for different film thicknesses are listed in Table 5. It can be seen that α depends on the thickness of the film and increases as the film thickness is decreased.

3.1.4.2. Ratio of first and second normal stress differences. Second normal stress difference N_2 was also computed from Eq. (16) for the same film thicknesses and shear rates as in Section 3.1.4.1. The ratio of N_1/N_2 is calculated and displayed in Fig. 7.

From Fig. 7 the results for all films at shear rates up 10^{10} s^{-1} show that the second normal stress difference N_2 always has the opposite sign of N_1 and is smaller than it. The ratio of $|N_1/N_2|$ ranges from 1 to 3. In shear ranges between $10^{10.5}$ and $10^{11.5} \text{ s}^{-1}$ however, some unusual behaviour is observed. We see that for a film thickness of 3.898 nm $|N_1/N_2|$ becomes smaller than 1 meaning that N_2 becomes larger than N_1 or for a film thickness of 2.924 nm where we observe an unexpectedly large ratio for $|N_1/N_2|$. At these shear ranges for the thinnest film of 0.975 nm N_1/N_2 becomes positive where N_1 and N_2 both are positive. Of course all these unusual behaviours at this shear range are explainable by seeing that this range of shear rate actually is the transient stage where N_1 and N_2 switch signs and N_1 becomes positive and N_2

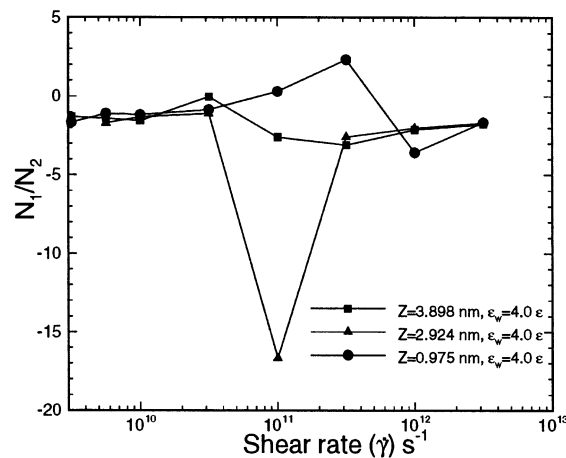


Fig. 7. Ratio of first to second normal stress difference for various film thicknesses. Wall–fluid interaction strength was $\varepsilon_w = 4\varepsilon$.

Table 6

Average bond length and bond angle for different film thicknesses. The result for all films are obtained at a shear rate of $10^{11.5} \text{ s}^{-1}$ and a wall–fluid interaction strength of $\varepsilon_w = 4\varepsilon$

Film thickness (nm)	Bond length (nm)	Bond angle (degree)
0.975	0.152585 ± 0.000022	109.1992 ± 0.0076
1.949	0.152716 ± 0.000023	109.2912 ± 0.0045
2.924	0.152772 ± 0.000022	109.3451 ± 0.0026
3.898	0.152814 ± 0.000022	109.4105 ± 0.0021
4.873	0.152821 ± 0.000021	109.4143 ± 0.0023
5.848	0.152835 ± 0.000021	109.4331 ± 0.0022
6.822	0.152844 ± 0.000020	109.4436 ± 0.0020
19.492	0.152885 ± 0.000020	109.5090 ± 0.0012

becomes negative. So at this stage we might expect some unusual values and signs for N_1/N_2 . However, after this transient stage we can see that $|N_1/N_2|$ is again about between 1 and 3 with N_2 having an opposite sign to N_1 .

3.1.5. Structural properties

The structural properties of the hexadecane molecule were examined for various film thicknesses at different shear rates. These properties included bond-length, bond-angle, end-to-end length $\langle R \rangle$ of the molecule, dihedral angle distribution, bond angle distribution and orientation parameter.

In the following sections we will investigate these properties and will discuss the effect of shear rate and film thickness on them.

3.1.5.1. The effect of the film thickness. The effect of the film thickness on the structural properties of the hexadecane molecule was studied for film thicknesses between 0.975 and 19.492 nm. The results for the average bond-length and bond angles are shown in Table 6 for various film thicknesses. From the values in Table 6 it can be seen that the average values of bond angle and bond length remain very close to their equilibrium values of $\theta_0 = 109.53^\circ$ and $r_0 = 0.153 \text{ nm}$. However, it can be seen that as the film thickness decreases the bonds are slightly compressed resulting in a small but clear decrease in bond length and bond angle.

The probability distribution of the dihedral angle (α) and bond angle (θ) were also computed for various film thicknesses. For all these simulations a shear rate of $10^{11.5} \text{ s}^{-1}$ was applied. The results for dihedral angle and bond angle are shown in Fig. 8 and Fig. 9, respectively. The measurements are averaged over all chains and over all the angles in one molecule. Dihedral angles $\alpha = 0$ and $\alpha = \pm 120^\circ$ are called ‘*trans*’ and ‘*gauche*’ angles, respectively. From Fig. 8 for dihedral angle it can be seen that probability is maximum at *trans* angles of $\alpha = 0$ and 360° where the torsional potential is minimum. Two other maxima can be seen in *gauche* angles at $\alpha = \pm 120^\circ$ where the torsional potential has secondary minima. The minimum probability is at $\alpha = 180^\circ$ where the torsional potential is a maximum followed by secondary minima at $\alpha = \pm 60^\circ$. This kind of dihedral angle probability distribution is generally expected from the RB model for torsional potential.

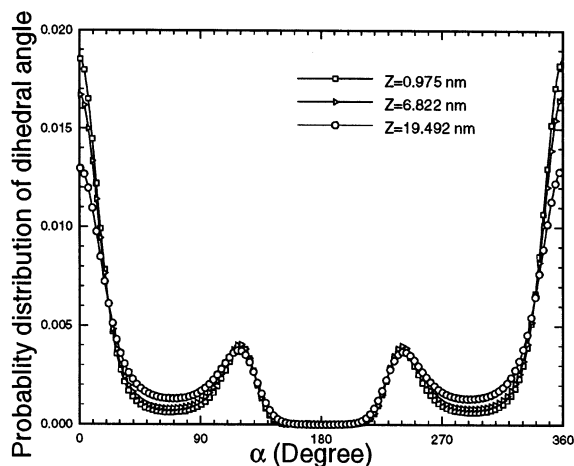


Fig. 8. Dihedral angle distribution for different film thicknesses. For all the simulations here, the shear rate was $10^{11.5} \text{ s}^{-1}$ and the wall–fluid interaction was $\epsilon_w = 4\epsilon$.

It can be seen from Fig. 8 that the film thickness has an effect on the dihedral angle distribution. Here the results are presented for three films. The thinnest film is only 2.5 segment diameters (roughly) and the largest film is about 50 segment diameters. It can clearly be seen there is a stronger tendency for the chains to be in the *trans* state in thinner films. However, as the film thickness is increased the portion of the *trans* conformations is decreased. There is also an increased preference for the dihedral angle to be in the secondary minima around $\alpha = \pm 60^\circ$. These changes in the dihedral angle distribution can be explained by the adsorption of the chains to the walls. For the chains adsorbed onto the walls the natural orientation is in the *trans* state where they can be parallel to the walls and keep their energy level in a minimum state. In

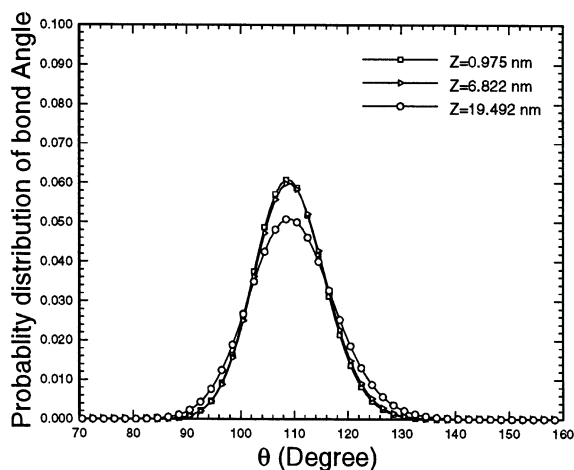


Fig. 9. Bond angle distribution for different film thicknesses. For all the simulations here the shear rate was $10^{11.5} \text{ s}^{-1}$ and the wall–fluid interaction was $\epsilon_w = 4\epsilon$.

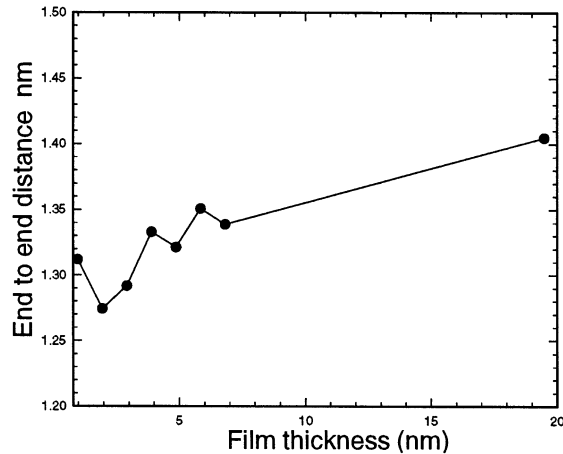


Fig. 10. Average end-to-end distance of the molecules against the film thickness. The results for all films are obtained at a shear rate of $10^{11.5} \text{ s}^{-1}$ and wall–fluid interaction strength of $\varepsilon_w = 4\varepsilon$.

thinner films these adsorbed chains make up a bigger portion of the total chains, hence a bigger portion of the dihedral angles can be found in the *trans* state. For thicker films a greater portion of the molecules are free in the middle part away from adsorption at the walls.

The molecules in the middle part are affected less strongly by the walls. This makes them more relaxed and therefore the *trans* conformations probability is decreased.

For the bond angle distribution it can be seen from Fig. 9 that there is a narrow distribution because of the stiff angular potential used here. The probability is highest close to its equilibrium value of 109.5° . The probability for angles deviating by $\pm 30\text{--}40^\circ$ from the equilibrium value virtually drops to zero. The results show that there is no significant change in bond angle distribution as the film thickness is increased from 0.975 to 6.822 nm. However, at the thickest film of 19.492 nm the bond angles are more relaxed and span over slightly larger angles. That is the reason why the average bond angle is the highest in this film thickness as it is seen in Table 6.

The effect of the film thickness was also investigated on the end-to-end distance for various film thicknesses. The results are illustrated in Fig. 10. Although, the end-to-end distance has an oscillatory behaviour with film thickness it seems that the general trend is that it increases as the film thickness is increased.

This is an indication that the hexadecane molecules are less stretched in thinner films. The decrease in the end-to-end distance at thinner film might seem at first sight somewhat contradictory with increase in *trans* percentage for thinner films. However, it can be explained by the strong attraction force from the walls which prevents the chains from aligning in a fully stretched orientation. Also the compression of the bond angles and bond lengths in thinner films, which was seen from the results in Table 6, further contributes to a decrease in the end-to-end vector length. It seems that two mentioned reasons have dominating effect on end-to-end distance.

One of the other important structural properties is the orientation of the chains with respect to the walls. To investigate this the square of the direction cosine ($\cos^2 \theta_z$) of the bond vectors

with respect to the Z axis (normal to the wall) was measured and its MD average was calculated over all the molecules and their bonds and over the time. For brevity we call $(\cos \theta_z)^2$ the orientation factor. A value close to zero for $(\cos \theta_z)^2$ is an indication that bonds are oriented close to parallel with respect to the walls and a value close to 1 shows that the bonds are mostly normal to the walls. The results for $(\cos \theta_z)^2$ are shown in Fig. 11 for various film thicknesses.

As can be seen from this figure the orientation of the bonds is more close to parallel. The values for $(\cos \theta_z)^2$ in Fig. 11 imply that molecular bonds make an average angle of about 60° with the positive side of the Z axis (normal to the walls) in the upper half of the flow region and the same angle with respect to the negative side of the Z axis in the lower half of the flow region. The measurements are at a high shear rate so the alignment of the molecules in the direction of flow makes the bonds more parallel to the walls. We can also see that this tendency for the bonds to line up parallel to the walls is stronger in thinner films especially in the thinnest film of 0.9746 nm. Simulations by Bitsanis and Hadziioannou [11] for flexible chains of model polymer melts in the equilibrium state showed that there was a preferential orientation parallel to the wall immediately next to the walls followed by a region of peak density where bonds tended to be normal to the walls. At distances further from the walls the bonds were oriented randomly. In our case however, since there are strong intramolecular potentials such as the bond angle and torsional potentials and because of the high shear rates the tendency of the bonds to align themselves parallel to the wall is stronger. But at intermediate thicknesses it still seems that there is a greater normal alignment in compare to the thickest and thinnest films. It seems that normal alignment of bonds in peak density region is the reason for this difference if Bitsanis and Hadziioannou's [11] results are considered here. A closer investigation of this problem perhaps by looking to the local bond orientation may give some insight to the problem.

3.1.5.2. The effect of the shear rate. The effect of the shear rate on the structural properties of the hexadecane molecules was also investigated over various shear rates ranging from $10^{9.5}$ to $10^{12.5} \text{ s}^{-1}$ for various film thicknesses. Again here we will have the results for average bond

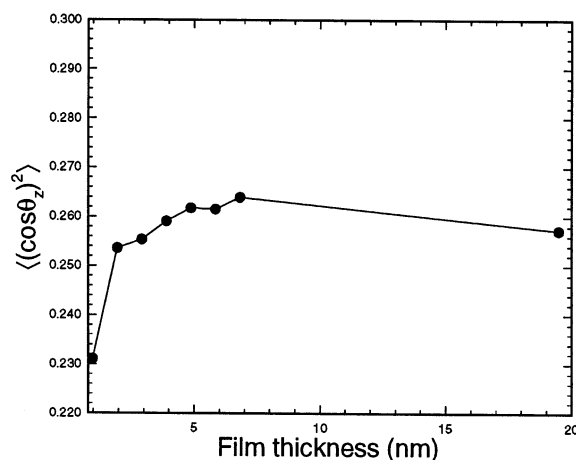


Fig. 11. Average orientation factor of the bonds with respect to the Z axis for various film thicknesses. The results for all films are obtained at a shear rate of $10^{11.5} \text{ s}^{-1}$ and wall–fluid interaction strength of $\varepsilon_w = 4\varepsilon$.

Table 7

Average bond length and bond angle for various shear rates. The results here are for a film with a thickness of 3.898 nm. Wall–fluid interactions strength was $\varepsilon_w = 4\varepsilon$

Log (shear rate (s^{-1}))	Bond length (nm)	Bond angle (degree)
9.5	0.152787 ± 0.000021	109.2502 ± 0.0018
9.75	0.152785 ± 0.000022	109.2441 ± 0.0015
10	0.152780 ± 0.000022	109.2343 ± 0.0025
10.5	0.152776 ± 0.000022	109.2453 ± 0.0030
11	0.152789 ± 0.000021	109.3085 ± 0.0027
11.5	0.152814 ± 0.000022	109.4105 ± 0.0021
12	0.152824 ± 0.000022	109.5719 ± 0.0018
12.5	0.152876 ± 0.000021	109.8738 ± 0.0062

length and bond angle for various shear rates for a film with a thickness of 3.898 nm. The results are given in Table 7. From the results in Table 7 it can be seen that the bond length remains almost constant and only an insignificant increase with the shear rate is observed. Nevertheless, the average bond angle is affected more and there is some increase in it at high shear rates, though it remains very close to the equilibrium value of 109.53° .

The probability distribution of the dihedral angle (α) and bond angle (θ) were also computed for various shear rates for a film with a thickness of 3.898 nm. The results for dihedral and bond angles are shown in Figs. 12 and 13, respectively. The measurements are averaged over all chains and over all the angles in one molecule. Examining the effect of shear rate on the dihedral angle distribution we can see that increasing the shear rate increases the probability of the dihedral angle being in the *trans* state while decreasing its probability of being in the *gauche* state. It is also interesting to see that the secondary minima at $\pm 60^\circ$ are increased with the shear rates. This is an indication that at higher shear rates chains more strongly prefer to be in the *trans*

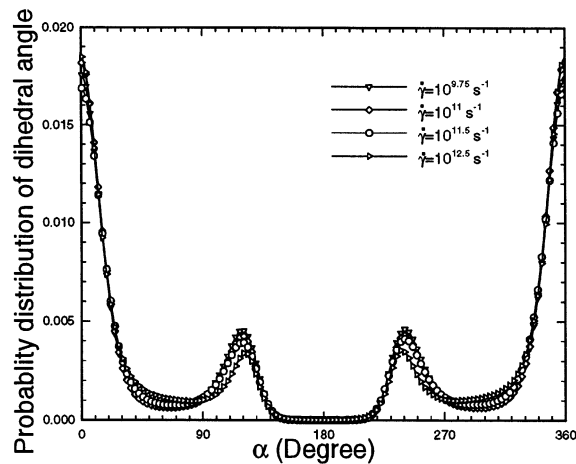


Fig. 12. Dihedral angle (α) distribution for various shear rates for a film with a thickness of 3.898 nm. Wall–fluid interaction strength was $\varepsilon_w = 4\varepsilon$.

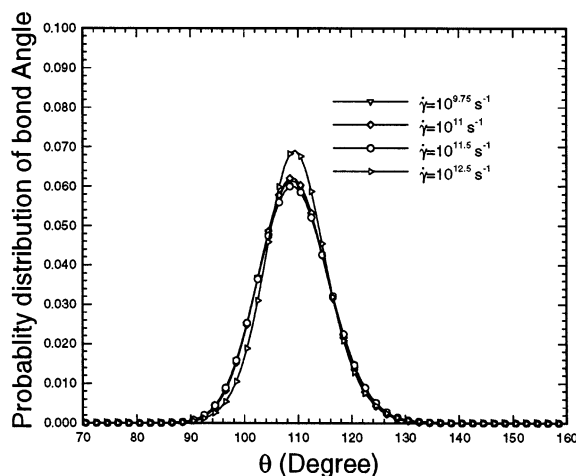


Fig. 13. Bond angle (θ) distribution for various shear rates for a film with a thickness of 3.898 nm. Wall–fluid interaction strength was $\varepsilon_w = 4\varepsilon$.

state or at angles close to it. It is interesting to see that the effect of increasing the shear rate is similar to making the film thinner. In Fig. 13 it can be seen that the bond angle distribution is in a relatively narrow range, as is expected from the stiff angular potential used here. The probability is highest close to its equilibrium value of 109.5° . The probability for angles deviating by ± 30 – 40° from the equilibrium value virtually drops to zero. It can be seen that there is not much change in the distribution as the shear rate is increased from low to moderately high shear rates. Only at the highest shear rate of $10^{12.5} \text{ s}^{-1}$ the distribution become narrower and the maximum shifts slightly to larger angles. This also can be confirmed by looking at the results in Table 7 where it can be seen that the average bond angle is the highest at $\dot{\gamma} = 10^{12.5} \text{ s}^{-1}$.

The average end-to-end distance $\langle R \rangle$ of the molecules was also calculated at various shear rates for films with different thicknesses. These results are plotted in Fig. 14. It can be seen that for thicker films of 2.924 and 3.898 nm, there is an increase in the end-to-end distance as we move from low shear rates to high shear rates. For these films however, there is a plateau with some decrease in $\langle R \rangle$ at shear rates 10^{11} – 10^{12} s^{-1} followed by a further increase at higher shear rates. For the thinnest film of 0.975 nm, except for the lower shear rates, the story is much the same. For this film at lower shear rates $\langle R \rangle$ is decreased as we increase the shear rates. At higher shear rates the behaviour is similar to that of the thicker films. The main reason for the increase in $\langle R \rangle$ is the unwinding of internal constraints such as the torsional and bond angles and also the elongation of the intramolecular bonds under the applied shear field. Interestingly, exactly the same behaviour was observed for the end-to-end distance in the simulation of bulk hexadecane by Chynoweth et al. [16]. At the thinnest film of 0.975 nm the story is a little different at lower shear rates. For this film the end-to-end distance $\langle R \rangle$ in general has the same trend though at low shear rates it almost remains constant while for thicker films at these shear rates $\langle R \rangle$ is increasing. For this film, examining the velocity profiles at different shear rates in Fig. 3 shows that some slip is present at low shear rates, and that it decreases with increasing the shear rate. This slip is one of the reasons for this different behaviour.

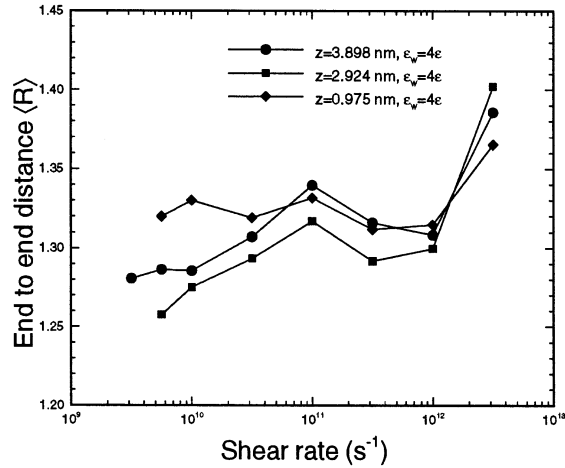


Fig. 14. Average end-to-end distance of the molecules for various shear rates for films with a thickness of 0.975, 2.924 and 3.898 nm. For all the simulations a wall–fluid interaction strength of $\epsilon_w = 4\epsilon$ was used. The error bars are all smaller than the symbols so they are not shown in the graph. Typical statistical error is $\sigma(\langle R \rangle) \approx 0.003$.

The average orientation factor of the bonds with respect to the Z axis $\langle(\cos \theta_z)^2\rangle$ was also monitored as a measure of their orientation, over various shear rates for the same film thicknesses of 0.975, 2.924 and 3.898 nm. The results are presented in Fig. 15. It can be clearly seen that tendency of the bonds to align parallel to the walls becomes stronger as the shear rate is increased. This tendency is stronger for thinner films as manifested by lower values for $\langle(\cos \theta_z)^2\rangle$.

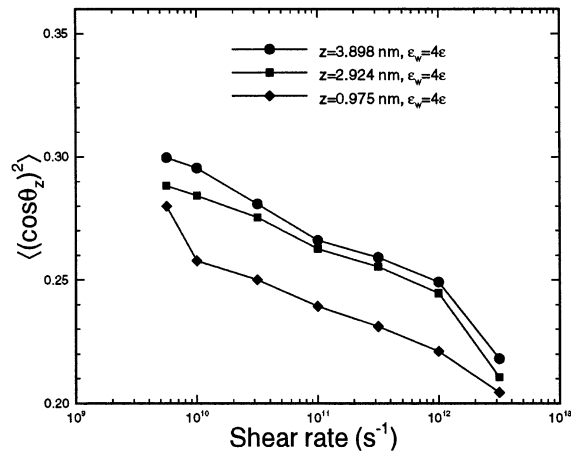


Fig. 15. Average direction cosine with respect to the Z axis $\langle(\cos \theta_z)^2\rangle$ against the shear rate for various film thicknesses. For all the simulations the wall–fluid interaction strength was $\epsilon_w = 4\epsilon$. The error bars are all smaller than the symbols so they are not shown here. Typical statistical error is $\sigma[\langle(\cos \theta_z)^2\rangle] \approx 0.001$.

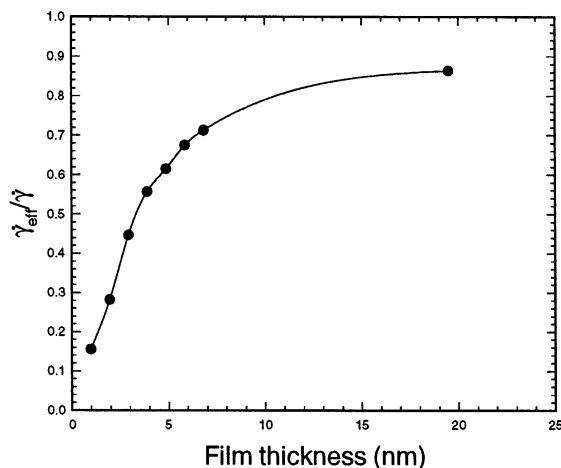


Fig. 16. Ratio of the effective shear rate to applied shear rate against the film thickness. The shear rate for all the data here was $10^{11.5} \text{ s}^{-1}$ and wall–fluid interaction strength was $\varepsilon_w = \varepsilon$.

3.2. Weakly adsorbing wall

In this section we will examine the rheological properties of hexadecane films confined between weakly adsorbing surfaces. These surfaces have a weaker interaction potential with the fluid molecules. In this case a wall–fluid interaction parameter $\varepsilon_w = \varepsilon$ is used. In the experiments, usually to achieve a surface with lower energy, mica surfaces are coated with a layer of octadecyltriethoxysilane (OTE) [7]. The result is a surface many times more weakly adsorbing than the mica itself. It is of great importance to see what happens to the confined sheared fluid with these low adsorbing surfaces. There are some theoretical predictions for the properties of polymer melts interacting with these kind of surfaces in shear flow [30]. It is useful to compare those theoretical predictions with the simulation findings.

3.2.1. Slip

One of the important characteristics of the shear flow between weakly adsorbing surfaces is the slip between the fluid and the wall. This problem is investigated in detail in our previous work [21]. To highlight the effect of slip and to quantify it, we calculated the effective shear rate ($\dot{\gamma}_{\text{eff}}$) inside the film from the velocity profiles and plotted the ratio of $\dot{\gamma}_{\text{eff}}/\dot{\gamma}$ against the film thickness and also against the applied shear rate $\dot{\gamma}$. The results are displayed in Fig. 16 and Fig. 17. It should be noted that values less than 1 for $\dot{\gamma}_{\text{eff}}/\dot{\gamma}$ indicate slip boundary conditions and a value of 1 indicates the non-slip condition. In Fig. 16 the shear rate for all the simulated systems was $10^{11.5} \text{ s}^{-1}$. It can be seen the slip is higher with thinner films and is decreased as we increase the film thickness. It seems that $\dot{\gamma}_{\text{eff}}/\dot{\gamma}$ goes to unity at thick enough films. It suggests that with a very thick film a non-slip boundary condition holds.

To show the shear rate dependence of slip, simulations at various shear rates were performed for a film thickness of 3.898 nm. Fig. 17 shows $\dot{\gamma}_{\text{eff}}/\dot{\gamma}$ against the shear rate for this film thickness. It can be seen that the slip is large at low shear rates with lower values for. As the shear rate

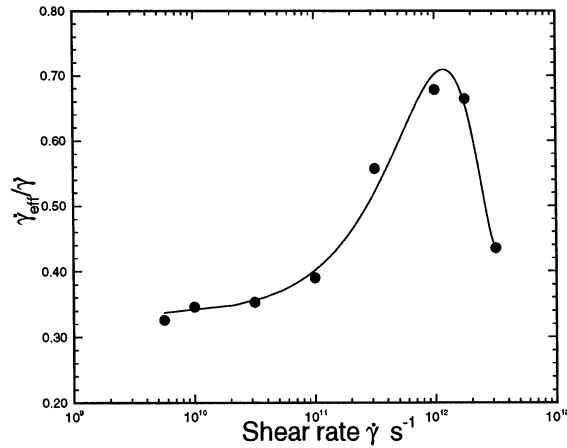


Fig. 17. Ratio of the effective shear rate to applied shear rate against applied shear rate. The film thickness for all the simulated points was 3.898 nm and wall–fluid interaction strength was $\varepsilon_w = \varepsilon$.

is increased, $\dot{\gamma}_{eff}/\dot{\gamma}$ is increased as an indication of decrease in the slip. However, $\dot{\gamma}_{eff}/\dot{\gamma}$ never reaches unity and there is a turning point at shear rates of around $10^{12} s^{-1}$. At this point the slip again increases and $\dot{\gamma}_{eff}/\dot{\gamma}$ drops as we increase the shear rate.

3.2.2. Viscosity and film thickness

The viscosity was examined for films with thicknesses ranging from 0.975 to 19.492 nm, at a shear rate of $10^{11.5} s^{-1}$ and with a wall–fluid interaction parameter $\varepsilon_w = \varepsilon$. The results are displayed in Fig. 18. It can be seen that the results are quite different from that with strongly adsorbing surfaces examined in Section 3.1.1. Here the viscosity is an increasing function of the film thickness. It can be seen from Fig. 16 that the behaviour of the viscosity is highly correlated

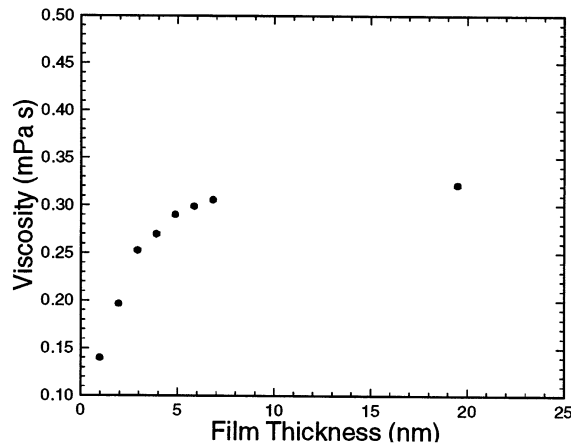


Fig. 18. Apparent viscosity of thin films of hexadecane for various film thicknesses sheared between weakly adsorbing surfaces with a wall–fluid interaction parameter $\varepsilon_w = \varepsilon$. For all the simulations the shear rate was $10^{11.5} s^{-1}$.

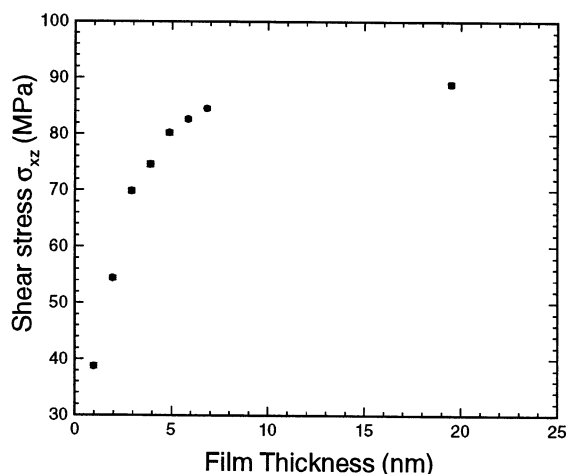


Fig. 19. Shear stress against film thickness for low adsorbing surfaces for various film thicknesses where for all the simulated systems $\varepsilon_w = \varepsilon$ and the shear rate was $10^{11.5} \text{ s}^{-1}$.

with the slip. Actually the main reason for the increase in viscosity is that as we increase the film thickness, slip is decreased and the ratio of the effective shear rate to the applied shear rate ($\dot{\gamma}_{\text{eff}}/\dot{\gamma}$) is increased which means that the inside of the film of fluid experiences higher shear rates that result in higher shear stresses. Fig. 19 shows how the shear stress changes with film thickness.

Since Eq. (15) is used for calculation of the viscosity based on the applied shear rate increasing the shear stress at the same applied shear rate will result in a higher viscosity as is seen in Fig. 18. It is interesting to see that the viscosity of thick films reaches about the same level of the viscosity with strongly adsorbing surfaces and at the same film thickness shown in Fig. 2. It implies that the viscosity at thick enough films is independent of the level of adsorption and the strength of the wall–fluid interaction. This is a significant conclusion which confirms that the adsorption is important if the portion of the adsorbed molecules is significant compared to the whole film.

3.2.3. Viscosity and shear rate

The viscosity was obtained over the same shear range as in Section 3.1.2 and for films with a thickness of 0.975, 2.924 and 3.898 nm. The results are shown in Fig. 20. As can be seen in this figure the viscosity basically remains constant at the thinnest film. For thicker films there is a slight shear thinning with a power law behaviour. Fitting the results to the power law in the form $\eta = A\dot{\gamma}^{-\alpha}$ of for different film thicknesses the measured values for α are listed in Table 8. It can be seen that the value of α is very small (close to zero) for the thinnest film. At thicker films although, α still remains much smaller than the typical values characteristic of non-Newtonian behaviour, it increases with film thickness. This can however, be explained by the lower slip present with thicker films.

In Fig. 21 shear stress σ_{xz} is plotted against the shear rate on a logarithmic scale. It can be seen that the shear stress is an increasing function of shear rate in the form of $\sigma_{xz} = A\dot{\gamma}^\alpha$. The

Table 8

The value of α at different film thicknesses for the power law dependence of viscosity to shear rate given by $\eta = A\dot{\gamma}^{-\alpha}$ for a low adsorbing surface with $\epsilon_w = \epsilon$

Film thickness (nm)	0.975	2.924	3.898
α	0.012	0.065	0.139

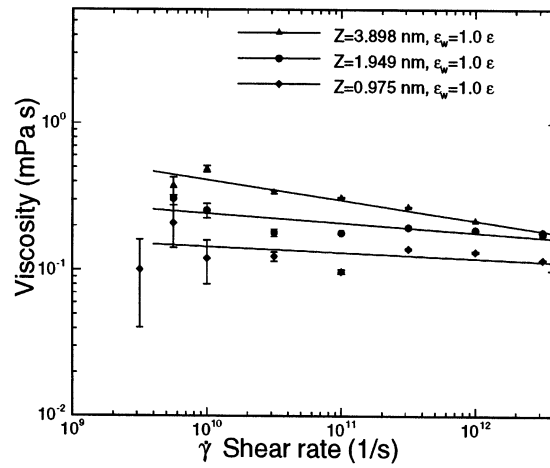


Fig. 20. Apparent viscosity against the shear rate in a logarithmic scale for three different film thicknesses for a low adsorbing surface with $\epsilon_w = \epsilon$.

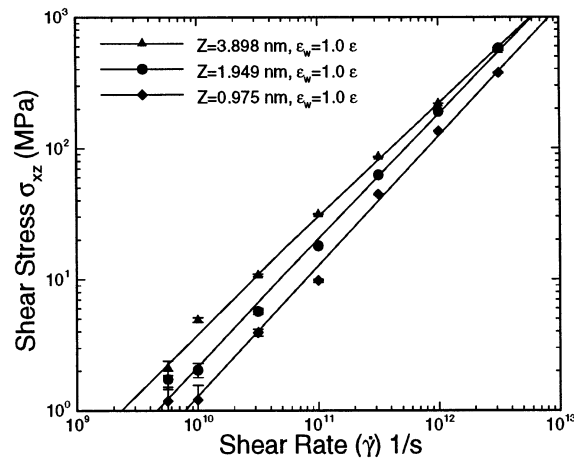


Fig. 21. Shear stress against the shear rate for three film thicknesses for a low adsorbing surface with $\epsilon_w = \epsilon$.

In Fig. 21 shear stress σ_{xz} is plotted against the shear rate on a logarithmic scale. It can be seen that the shear stress is an increasing function of shear rate in the form of $\sigma_{xz} = A\dot{\gamma}^\alpha$. The value of α is almost 1 for films with a thickness of 0.975 and 2.924 nm. For the thicker film of 3.898 nm, as might be also inferred from the viscosity data α is slightly smaller, about 0.86.

These results suggest that with these weakly adsorbing surfaces the response of the fluid to the applied shear rate is closer to Newtonian while at strongly adsorbing surfaces the response is non-linear and non-Newtonian. It is a very interesting phenomenon that the shear response of the same fluid at these thin films can be changed from Newtonian to non-Newtonian by manipulating the surface properties. However, experimental work is needed in this area to confirm these conclusions. Theoretical works by Subbotin et al. [30] on the shear response of polymer melts confined between weakly adsorbing surfaces support our findings. They have defined two characteristic shear rates $\dot{\gamma}_1$ and $\dot{\gamma}_2$. The amount of slip is large when $\dot{\gamma} < \dot{\gamma}_1$ and when $\dot{\gamma}_1 < \dot{\gamma} < \dot{\gamma}_2$ slip decreases and for shear rates $\dot{\gamma} > \dot{\gamma}_2$ the slip becomes negligible. According to their theoretical analysis the shear stress increases with shear rate as $\dot{\gamma}$ and viscosity remains constant for the shear rates in the range of $\dot{\gamma} < \dot{\gamma}_2$. However, they predict a shear thinning effect at shear rates higher than $\dot{\gamma}_2$. Our findings fit in well with theoretical prediction of Subbotin et al. [30] except at high shear rates. Considering their analogy and our results it seems that the first characteristic shear rate is at $\dot{\gamma}_1 \approx 10^{9.75} \text{ s}^{-1}$ or somewhat lower. However, we do not reach the second characteristic shear rate $\dot{\gamma}_2$ and increasing the shear rate beyond 10^{12} s^{-1} results in further increase in the slip. Whether this is the result of the specific model we have used here with relatively short chains (in comparison to long polymer melt chains), or whether it is a fault in the theoretical prediction, is not known. It seems this matter needs more investigation at high shear rates, maybe through experiments or more simulations with longer chains. We think however, that at shear rates lower than 10^{12} s^{-1} that the simulation and theoretical results agree well.

4. Conclusions

In this paper we investigated the shear response of ultrathin films of hexadecane at different wall adsorption limits. It was demonstrated that the wall properties greatly affect the response of these thin films to the applied shear. With strongly adsorbing surfaces the viscosity is enhanced in very thin films, although in thicker films the viscosity remains fairly constant. The non-linear response to shear is observed by producing the flow curves for different film thicknesses. These indicate that viscosity obeys a power law where the exponent is dependant on the film thickness and increases in absolute value as the film thickness is decreased. The normal stress difference effect was also observed. It was shown that N_1 also obeys a power law behaviour that depends on the film thickness at high shears. It was seen that a very large normal stress difference can be produced at high shear rates. This shows that these thin films can endure very large normal pressures and high shear stresses at the same time. The effects of the film thickness and shear rates also were examined on the structural properties of the hexadecane molecules. It seems that the parallel orientation of the molecules is enhanced at thinner films and at higher shear rates. The molecules become more stretched as the shear rate is increased.

Changing the wall adsorption strength brings about some interesting results which are different from those with a strongly adsorbing surface. In this case the slip between the confined film and the surfaces plays an important role. It can be seen that the slip is both dependant on the shear rate and the film thickness. Actually, it results in an unexpected behaviour for the viscosity. First of all the viscosity is increased as the film thickness is increased. This is the direct result of decrease in the wall slip at thicker films. Secondly, as can be seen from the viscosity and shear stress data, the shear response of these films, especially at thinner films, is very close to Newtonian. This is a significant finding showing how important the surface properties are in the shear response of the these thin films. These findings, which are also confirmed partially by theoretical predictions, need more experimental examination. If confirmed, it can have significant applications in tribology, polymer processing coating and other surface related areas.

Acknowledgements

We gratefully acknowledge the support of an Australian Research Scheme grant for this work. We also wish to thank Professor N. Phan-Thien for providing us with generous time on the computing facility of the Sydney Distributed Computing Laboratory (SyDCom).

References

- [1] J.N. Israelachvili, *Colloid Polym. Sci.* 264 (1986) 1060.
- [2] J.N. Israelachvili, *Colloid Interface Sci.* 119 (1987) 194.
- [3] D.Y.C. Chan, R.G. Horn, *J. Chem. Phys.* 83 (1985) 5311.
- [4] H.K. Christenson, D.W.R. Gruen, G. Horn, J.N. Israelachvili, *J. Chem. Phys.* 87 (1987) 1834.
- [5] J. Van Alsten, S. Granick, *Phys. Rev. Lett.* 61 (1988) 2570.
- [6] G. Carson, H.W. Hu, S. Granick, *Tribology Trans.* 35 (1992) 405.
- [7] J. Peanasky, L.L. Gai, S. Granick, *Langmuir* 10 (1994) 3874.
- [8] H.W. Hu, G.A. Carson, S. Granick, *Phys. Rev. Lett.* 66 (1991) 2758.
- [9] A. Jabbarzadeh, J.D. Atkinson, R.I. Tanner, *J. Non-Newtonian Fluid Mech.* 69 (1997) 169.
- [10] P.A. Thompson, G.S. Grest, *Phys. Rev. Lett.* 68 (1992) 3448.
- [11] I. Bitsanis, G. Hadziioannou, *J. Chem. Phys.* 92 (1990) 3827.
- [12] I. Bitsanis, C. Pan, *J. Chem. Phys.* 99 (1993) 5520.
- [13] E. Manias, G. Hadziioannou, I. Bitsanis, G. Ten Brinke, *Europhys. Lett.* 24 (1993) 99.
- [14] A. Berker, S. Chynoweth, U.C. Klomp, Y. Michopoulos, *J. Chem. Soc. Faraday Trans.* 88 (1992) 1719.
- [15] S. Chynoweth, Y. Michopoulos, *Mol. Phys.* 81 (1994) 133.
- [16] S. Chynoweth, R.C. Coy, Y. Michopoulos, *Proc. Inst. Mech. Eng.* 209 (1995) 243.
- [17] S. Chynoweth, U.C. Klomp, L.E. Scales, *Comput. Phys. Commun.* 62 (1991) 297.
- [18] P.J. Davis, D.J. Evans, G.P. Morriss, *J. Chem. Phys.* 97 (1992) 616.
- [19] J.P. Ryckaert, A. Bellemans, *Chem. Phys. Lett.* 30 (1975) 123.
- [20] J.H.R. Clarke, D. Brown, *Computer simulation of polymers*, Longman, New York, 1994, pp. 47–90.
- [21] A. Jabbarzadeh, *Molecular dynamics simulation of thin liquid films*, PhD thesis, University of Sydney, 1997.
- [22] S.A. Somers, H.T. Davis, *J. Chem. Phys.* 96 (1992) 5389.
- [23] P. van der Ploeg, J.C. Berendsen, *J. Chem. Phys.* 76 (1982) 3271.
- [24] A. Jabbarzadeh, J.D. Atkinson, R.I. Tanner, *Comput. Phys. Commun.* 107 (1997) 123.
- [25] R.I. Tanner, *Engineering Rheology*, Oxford University Press, Oxford, 1985.

- [26] R.B. Bird, R.C. Armstrong, O. Hassager, *Dynamics of Polymeric Liquids*, vol. 1, Wiley-Interscience, London, 1987.
- [27] M. Doi, S.F. Edwards, *The Theory of Polymer Dynamics*, Clarendon Press, Oxford, 1986.
- [28] S. Bair, *Rheol Acta*. 35 (1996) 13.
- [29] A. Subbotin, A. Semenov, G. Hadziioannou, G. ten Brinke, *Macromolecules* 28 (1995) 1511.
- [30] A. Subbotin, A. Semenov, G. Hadziioannou, G. ten Brinke, *Macromolecules* 28 (1995) 3898.